Pharm Res (2021) 38:113–125
https://doi.org/10.1007/s11095-021-03003-1

RESEARCH PAPER

Participation of Monocarboxylate Transporter 8, But Not P-Glycoprotein, in Carrier-Mediated Cerebral Elimination of Phenytoin across the Blood-Brain Barrier

Ryuta Jomura[1] • Shin-ichi Akanuma[1,2] • Björn Bauer[2] • Yukiko Yoshida[1] • Yoshiyuki Kubo[1] • Ken-ichi Hosoya[1]

Received: 7 July 2020 / Accepted: 9 December 2020 / Published online: 1 February 2021

ABSTRACT

Purpose In this study, we investigated in detail the transport of phenytoin across the blood-brain barrier (BBB) to identify the transporter(s) involved in BBB-mediated phenytoin efflux from the brain.

Methods We evaluated the brain-to-blood efflux transport of phenytoin *in vivo* by determining the brain efflux index (BEI) and uptake in brain slices. We additionally conducted brain perfusion experiments and BEI studies in P-glycoprotein (P-gp)-deficient mice. In addition, we determined the mRNA expression of monocarboxylate transporter (MCT) in isolated brain capillaries and performed phenytoin uptake studies in MCT-expressing *Xenopus* oocytes.

Results [^{14}C]Phenytoin brain efflux was time-dependent with a half-life of 17 min in rats and 31 min in mice. Intracerebral pre-administration of unlabeled phenytoin attenuated BBB-mediated phenytoin efflux transport, suggesting carrier-mediated phenytoin efflux transport across the BBB. Pre-administration of P-gp substrates in rats and genetic P-gp deficiency in mice did not affect BBB-mediated phenytoin efflux transport. In contrast, pre-administration of MCT8 inhibitors attenuated phenytoin efflux. Moreover, rat MCT8-expressing *Xenopus* oocytes exhibited [^{14}C]phenytoin uptake, which was inhibited by unlabeled phenytoin.

Conclusion Our data suggest that MCT8 at the BBB participates in phenytoin efflux transport from the brain to the blood.

✉ Shin-ichi Akanuma
akanumas@pha.u-toyama.ac.jp

[1] Department of Pharmaceutics, Graduate School of Medicine and Pharmaceutical Sciences, University of Toyama, 2630 Sugitani, Toyama 930-0194, Japan

[2] Department of Pharmaceutical Sciences, College of Pharmacy, University of Kentucky, 800 S Limestone, Lexington, Kentucky 40536-0230, USA

KEY WORDS blood-brain barrier · MCT8 · monocarboxylate transporter · phenytoin · P-glycoprotein

ABBREVIATIONS

ABC	ATP-binding cassette
BBB	Blood-brain barrier
BEI	Brain efflux index
BCRP	Breast cancer resistance protein
BSP	Bromosulfophthalein
CEF	Cerebral extracellular fluid
cDNA	Complementary DNA
cRNA	Complementary RNA
CYP	Cytochrome P450
DHEAS	Dehydroepiandrosterone-3-sulfate
HEPES	4-(2-hydroxyethyl)-1-piperazine ethanesulfonic acid
MCT	Monocarboxylate transporter
MRP	Multidrug resistance-associated protein
n	Group sizes
P-gp	P-glycoprotein
S.D.	Standard deviation
SNP	Single nucleotide polymorphism
X	*Xenopus*

INTRODUCTION

Phenytoin (5,5-diphenylhydantoin) is a widely prescribed medication for the treatment of tonic–clonic and focal seizures in epilepsy patients. The key pharmacological mechanism of action for phenytoin is use-dependent blockade of archetypal voltage-gated sodium channels in neurons (1). Following its introduction as an anticonvulsant drug in 1938, phenytoin exhibited a rapid market penetration, and it was distributed worldwide by 1940. Around 1960, phenytoin was used for

treating status epilepticus for the first time (2). Because of this historical background, phenytoin is widely used for the pharmacotherapy of epilepsy. However, approximately 30% of epilepsy patients experience seizures that cannot be controlled with anti-seizure drugs; consequently, they suffer from refractory epilepsy (3). Therefore, for overcoming drug-resistant seizures, it is imperative that epilepsy pharmacotherapy with anti-seizure drugs such as phenytoin is improved.

Phenytoin follows non-linear pharmacokinetics, based on cytochrome P450 (CYP) 2C9 and CYP2C19 in the liver, which convert phenytoin to its primary metabolite 5-(4′-hydroxyphenyl)-5-phenylhydantoin (4). Studies suggest that among the enzymes involved, CYP2C9 is the major metabolizing enzyme responsible for phenytoin blood levels and, thus, the development of phenytoin-induced toxicity (5, 6).

For phenytoin to be therapeutically active, it has to distribute from the circulating blood into the brain across the blood-brain barrier (BBB); therefore, the transport and distribution of phenytoin need to be considered. Cornford *et al.* performed brain uptake index studies and provided direct evidence for the blood-to-brain influx transport of phenytoin in neonate and adult rats (7). Nevertheless, evidence demonstrating the brain-to-blood efflux transport of phenytoin is lacking. Since unbound drug concentration in the brain interstitial fluid depends on the net transport balance of both influx and efflux transport across the BBB (8), understanding phenytoin efflux transport across the BBB would help in estimating the phenytoin levels, thus, predicting the pharmacological and toxicological effects of phenytoin.

Multiple plasma membrane transporters at the BBB contribute to drug brain distribution. For example, facilitative glucose transporter 1 and monocarboxylate transporter (MCT) 1 are involved in the blood-to-brain influx transport of D-glucose and L-lactate, respectively (9). Data from other studies demonstrate the active transport of several cationic drugs, such as pyrilamine (10), from the blood to the brain across the BBB through unidentified transport system(s). In addition, several ATP-binding cassette (ABC) transporters, such as P-glycoprotein (P-gp/MDR1 in humans; P-gp/mdr1a and mdr1b in mice), breast cancer resistance protein (BCRP), and multidrug resistance-associated protein (MRP), that are located in the luminal membrane of the brain capillary endothelium limit drugs from entering the brain (9). Among these ABC transporters, phenytoin has been considered a P-gp substrate (11, 12). It has been reported that MCT8, an orphan MCT, is expressed at the BBB (13, 14) and that it accepts desipramine, which is a cationic drug similar to phenytoin (15). On the basis of these studies, it is considered that several plasma membrane transporters and transport systems participate in the transport of phenytoin across the BBB.

Thus, the objective of this study was to investigate in detail the kinetics of phenytoin transport across the BBB. To examine phenytoin efflux transport across the BBB and elucidate which transporters contribute to the phenytoin efflux, we utilized intracerebral microinjections of phenytoin to determine the brain efflux index (BEI) in male animals (16). In addition to the rat study, for elucidating the character of phenytoin efflux transport across the BBB, we performed a mouse study including *in vivo* BBB-mediated influx and efflux transport in P-gp knockout mice to evaluate whether P-gp participates in phenytoin transport at the BBB. Data from these *in vivo* studies suggest that P-gp does not contribute to phenytoin efflux transport across the BBB. Our data from MCT-expressing *Xenopus* (*X.*) oocytes suggest that orphan MCTs could be involved in phenytoin efflux transport.

MATERIALS AND METHODS

Reagents and Animals

5,5-Diphenylhydantoin, [4-^{14}C]- ([^{14}C]phenytoin; 55 mCi/mmol) and mannitol, D-[1-^{3}H]- ([^{3}H] D-mannitol; 12.3 Ci/mmol), a BBB-impermeable marker, were purchased from PerkinElmer (Waltham, MA, USA). Pentobarbital sodium salt solution was purchased from Kyorin Seiyaku (Tokyo, Japan). Unlabeled phenytoin was obtained from FUJIFILM Wako Pure Chemicals Industries (Osaka, Japan). Bromosulfophthalein (BSP), disodium salt hydrate, bovine serum albumin (BSA), desipramine hydrochloride, and PSC833 were obtained from Merck (Darmstadt, Germany). MK-571 was purchased from Cayman Chemical (Ann Arbor, MI, USA). All other chemicals were commercially available and of analytical grade.

The animal experiments performed in this study were approved by the Animal Care Committee of the University of Toyama (#A2017PHA-5 and #A2017PHA-6; Principal Investigator: K. Hosoya) and by the University of Kentucky Institutional Animal Care and Use Committee (Protocol #2014–1234; Principal Investigator: B. Bauer). Male Wistar/ST rats (average of approximately 200 g per animal) and regular FVB/NTcl mice (average of approximately 18 g per animal) were obtained from Japan SLC (Hamamatsu, Japan) and CLEA Japan (Tokyo, Japan) and maintained in a controlled environment (temperature: 23°C; humidity: 40%–50%; 12/12 h dark/light cycle). Male P-gp-deficient, *mdr1a/1b* knockout (FVB.129P2-Abcb1a^{tm1Bor}Abcb1b^{tm1Bor}), and wild-type FVB/NTac mice (7–9 weeks) were obtained from Taconic Biosciences (Germantown, NY, USA) and housed in a temperature- and humidity-controlled vivarium (temperature: 23°C; humidity: 60%–65%; 10/14 h dark/light cycle). Mature female *X. laevis* frogs were obtained from Kato-S-Science (Chiba, Japan) and maintained in a controlled environment (temperature: 15°C; humidity: 50%; 12/12 h dark/light cycle).

BEI

To evaluate drug elimination from the brain into the blood across the rat BBB, we performed the BEI method (16). The rats were anesthetized using a 50 mg/kg sodium-pentobarbital *i.p.* injection and fixed in a stereotaxic frame (SR-5R; Narishige, Tokyo, Japan). Each animal received 0.5 μL of test solution containing [^{3}H]D-mannitol (BBB integrity marker; 0.05 μCi/0.5 μL = 8.14 μM) and [^{14}C]phenytoin (0.01 μCi/0.5 μL = 364 μM) dissolved in an *in vivo* administration buffer (122 mM NaCl, 25 mM $NaHCO_3$, 10 mM D-glucose, 10 mM 4-(2-hydroxyethyl)-1-piperazine ethanesulfonic acid (HEPES), 3 mM KCl, 0.4 mM K_2HPO_4, 1.4 mM $CaCl_2$, and 1.2 mM $MgSO_4$; pH 7.4). The test solution was administered via microinjection into the parietal cortex area 2 (Par 2) region of the rat cerebrum. For inhibition studies, an inhibitor solution (50 μL) was pre-administered into the Par2 region 5 min prior to the administration of the isotope-containing test solution. The anesthetized rats were euthanized by decapitation at designated time points, the ipsilateral and contralateral brain hemispheres were collected and dissolved in 2 M NaOH at 55°C for 3 h, and the solubilized sample was subsequently mixed with Hionic-Fluor liquid scintillation cocktail (PerkinElmer).

In BEI studies on mice, the animals were anesthetized using a 40 mg/kg sodium-pentobarbital *i.p.* injection and fixed in a small animal stereotaxic frame (David Kopf Instruments, CA, USA). Each mouse was administered 0.3 μL of test solution containing [^{3}H]D-mannitol (0.096 μCi/0.3 μL = 26.0 μM) and [^{14}C]phenytoin (0.019 μCi/0.3 μL = 1.15 mM) via microinjection into the somatosensory 2 (S2) region of the mouse cerebrum, as described previously (17). The anesthetized mice were euthanized by decapitation at designated time points, and the ipsilateral and contralateral brain hemispheres were collected and dissolved in Solvable™ (PerkinElmer) at 50°C for at least 3 h and, subsequently, mixed with Ultima Gold liquid scintillation cocktail (PerkinElmer).

The sample radioactivity from [^{3}H]D-mannitol and [^{14}C]phenytoin was measured using an AccuFLEX LSC-7400 (Aloka, Tokyo, Japan) or LS-6500 (PerkinElmer) liquid scintillation counter. The BEI was calculated according to Eq. (1), and the percentage of [^{14}C]phenytoin remaining in the ipsilateral hemisphere (100 − BEI) was determined using Eq. (2):

$$\mathrm{BEI}(\%) = \frac{[^{14}\mathrm{C}]\text{Phenytoin undergoing efflux at the BBB}}{[^{14}\mathrm{C}]\text{Phenytoin injected into the brain}} \times 100 \quad (1)$$

$$100-\mathrm{BEI}(\%) = \frac{[^{14}\mathrm{C}]\text{Phenytoin/BBB}-\text{impermeable marker in the brain}}{[^{14}\mathrm{C}]\text{Phenytoin/BBB}-\text{impermeable marker in the injectate}} \times 100 \quad (2)$$

Uptake Experiments in Rat Brain Slices

Rat brain slices (400 μm thick) were prepared as described previously (18). The brain slices were pre-incubated with oxygenated cerebral extracellular fluid buffer (122 mM NaCl, 25 mM $NaHCO_3$, 10 mM D-glucose, 10 mM HEPES, 3 mM KCl, 0.4 mM K_2HPO_4, 1.4 mM $CaCl_2$, and 1.2 mM $MgSO_4$; pH 7.4) for 5 min at 37°C. Subsequently, [^{14}C]phenytoin was added to the uptake buffer to a final concentration of 0.2 μCi/mL (= 3.64 μM). At designated time points, the slices were removed from the uptake buffer, dried on filter paper, weighed, and solubilized by adding 1 mL of 1 N NaOH solution. Simultaneously, samples of the uptake buffer were collected, and [^{14}C]phenytoin radioactivity was measured using an AccuFLEX LSC-7400 liquid scintillation counter.

[^{14}C]Phenytoin uptake in the rat brain slices was expressed as the slice/medium ratio (mL/g brain), which is defined as the [^{14}C]phenytoin amount in the slice (dpm/g brain) divided by the [^{14}C]phenytoin concentration in the uptake buffer (dpm/mL). Because the adsorbed volume of water is 0.125 mL/g brain (16), the [^{14}C]phenytoin distribution volume in rat brain ($V_{d,\ brain}$) was obtained using Eq. (3):

$$V_{d,\ brain} = \text{Steady}-\text{state}\,[^{14}\mathrm{C}]\text{phenytoin slice/medium ratio} - 0.125 \quad (3)$$

Mouse *In Situ* Brain Perfusion

To examine the blood-to-brain transport of [^{14}C]phenytoin in the mice, we performed *in situ* brain perfusion, as described previously (19). Dulbecco's Phosphate Buffered Saline (DPBS; HyClone, Logan, UT, USA) supplemented with 5 mM D-glucose was used as the perfusion buffer, which contained [^{14}C]phenytoin (0.15 μCi/mL = 2.73 μM) and [^{3}H]D-mannitol (0.5 μCi/mL = 40.7 nM; vascular marker). A 150 mL glass syringe (Becton Dickinson, Franklin Lakes, NJ, USA) with perfusion buffer was placed in a Harvard Apparatus Pump 33 (Harvard Apparatus, Holliston, MA, USA), and a Surflo winged infusion catheter (needle: 19G × 3/4″, tubing: 30 cm/12″, Terumo, Vaughan, Ontario, Canada) was connected to it. The mice were fully anesthetized using a 50 mg/kg sodium-pentobarbital *i.p.* injection, the thorax was opened, the descending aorta was clamped, and a small cut was made on the right ventricle. The mice were perfused through the left ventricle for 2 min at a perfusion rate of 2.5 mL/min. Following the perfusion, the anesthetized mice were euthanized by decapitation, the brains collected, and the hemispheres separated. The brain cortical tissue was solubilized in Solvable® at 50°C overnight, and the radioactivity was measured using an LS-6500 liquid scintillation counter. The [^{3}H]D-mannitol vascular volume (V_V) was calculated using Eq. (4); the [^{14}C]phenytoin brain uptake space was calculated

using Eq. (5), and the unidirectional uptake transfer constant, K_{in}, (μL/(s·g brain) was determined using Eq. (6), assuming that the phenytoin transport was linear at the 2 min time point.

$$V_v = Q_{tot}/C_p \quad (4)$$

$$\text{Brain uptake space} = \left(Q_{tot} - V_v \times C_p\right)/C_p \quad (5)$$

$$k_{in} = \left(Q_{tot} - V_v \times C_p\right)/\left(t \times C_p\right) \quad (6)$$

Q_{tot}: total amount of radiotracer in the brain; C_p: concentration of the radiotracer in the perfusate; t: perfusion time.

Isolation of Brain Capillaries, Brain, Liver, and Kidney

The rats and mice were anesthetized by *i.p.* injection of 50 mg/kg sodium-pentobarbital solution. After the animals were euthanized, their brains, livers, and kidneys were collected and subsequently washed with PBS (−). These tissues were minced and used for total RNA isolation.

Brain capillaries were isolated as described previously with minor modifications (20). Briefly, 4 brains from the anesthetized rats or 10 brains from the anesthetized mice were collected in an ice-cold Isolation Buffer (137 mM NaCl, 8.1 mM Na_2HPO_4, 1.5 mM KH_2PO_4, 2.7 mM KCl, 1.8 mM $CaCl_2$, 10 mM D-glucose, and 2.0 mM sodium pyruvate; pH 7.4). After removing the white matter and meninges, the brains were homogenized in the Isolation Buffer, mixed with dextran (final concentration: 16%; Thermo Fisher Scientific, Waltham, MA, USA), and centrifuged at 4500×g for 20 min at 4°C. The pellet was suspended in 1% BSA-containing Isolation Buffer and filtered through a 210 μm nylon mesh (Kyoshin Rikoh, Tokyo, Japan). The flow-through was passed over a 30 μm CellStrainer (pluriSelect Life Science, Leipzig, Germany), and the brain capillaries trapped on the CellStrainer membrane were collected using 1% BSA-containing Isolation Buffer. The brain capillaries were washed twice with Isolation Buffer and used for total RNA isolation or Western blot analysis.

Total RNA Isolation and Reverse Transcription-Polymerase Chain Reaction (RT-PCR)

Total RNA in the rat or mouse brain capillaries, brain, liver, and kidney was isolated using the TRIzol reagent (Thermo Fisher Scientific). cDNA was synthesized from total RNA using oligo dT primer (Thermo Fisher Scientific) and ReverTra Ace (Toyobo, Osaka, Japan). The cDNA samples were used for PCR with ExTaq DNA polymerase (Takara Shuzo, Kyoto, Japan). The sequences of the primers used to detect the amplified products are shown in Table I. The thermal protocol consisted of 2 min at 94°C for the rat study or 98°C for the mouse study, followed by 30 cycles for β-actin and MCT5, MCT7, MCT8, MCT10, MCT11, MCT12, and MCT14 or 35 cycles for MCT9 and MCT13 of 10 s at 98°C, 1 min at 57°C for the rat study or 30 s at 60°C for the mouse study, and 2 min at 72°C for the rat study or 1 min at 72°C for the mouse study, and, subsequently, 10 min at 72°C. The above PCR conditions, such as cycling numbers and temperatures, were selected on the basis of the bands detected in the respective positive controls. The samples resulting from the RT-PCR of total RNA without reverse transcriptase were used as negative controls. The amplified products were separated by agarose gel electrophoresis, stained with ethidium bromide solution (0.6 μg/mL), and visualized under UV light.

Western Blot Analysis

The crude membrane fraction of isolated rat brain capillaries and liver was prepared following our previous report (21) with minor modifications. Briefly, the pellet of rat brain capillaries and rat liver was homogenized at 4°C in suspension buffer (pH 7.4), which was composed of 1 mM ethylenediaminetetraacetic acid, 1 mM ethylene glycol tetraacetic acid, 10 mM 4-(2-hydroxyethyl)-1-piperazineethanesulfonic acid-NaOH, and 320 mM sucrose, by the nitrogen cavitation technique (850 psi) for 20 min. The homogenate was centrifuged at 10,000×g for 20 min at 4°C; subsequently, the supernatant was additionally centrifuged at 100,000×g for 60 min at 4°C. Crude membrane fraction of each tissue was obtained as suspension of the resulting pellet in the suspension buffer, and its concentration was determined by DC protein assay kit II (BIO-RAD, Hercules, CA, USA). The proteins (25 μg) were electrophoresed onto 10% sodium dodecyl sulfate–polyacrylamide gel and, subsequently, electroblotted onto an Amersham Hybond P membrane (Cytiva, Tokyo, Japan). The membranes for MCT8 and Na^+, K^+-ATPase α1 protein detection were treated with 5% non-fat dry milk and 0.1% Tween-20-containing tris-buffered saline (25 mM Tris-HCl and 125 mM NaCl, pH 7.4) for 1 h at 20°C and for approximately 12 h at 4°C, respectively. The blocked membrane was incubated with rabbit-derived anti-MCT8 (20676–1-AP; Proteintech, Rosemont, IL, USA) for approximately 12 h at 4°C or mouse-derived anti-Na^+, K^+-ATPase α1 antibodies (05–369; Merck) for 2 h at 20°C. The detection of Na^+, K^+-ATPase α1 proteins was utilized for the loading control of the crude membrane fraction (21). Following incubation with horseradish peroxidase-conjugated anti-rabbit or anti-mouse immunoglobulins, the proteins on the membrane were visualized using a SuperSignal West Atto Ultimate Sensitivity Chemiluminescent Substrate (Thermo Fisher Scientific).

Table I Conditions for RT-PCR

Target	SLC gene name	GeneBank Accession #	Primer (Upper, sense; Lower, antisense)	Expected Size
MCT5	Slc16a4	NM_001013913	5′-gct acc tgg ttt ggg gtc tg-3′ 5′-cca gaa aga aca gcc atc cca g-3′	981 bp
MCT7	Slc16a6	NM_198760	5′-ttg ttc cag ggc caa tgt gt-3′ 5′-ccc caa acc aga gac gat cc-3′	361 bp
MCT8 (rat)	Slc16a2	NM_147216	5′-tcc tgc tcc tgg gct tga tgt cta tg-3′ 5′-acg aag aaa agg atc aca gcc cca at-3′	310 bp
MCT8 (mouse)	Slc16a2	NM_009197.2	5′-tcc tgc tcc tgg gct tga tgt cca tg-3′ 5′-acg aag aaa agg atc aca gct cca at-3′	310 bp
MCT9	Slc16a9	XM_017588050	5′-ggt acc ctc aca atg ggg ttt cag aag-3′ 5′-gaa ttc ccc tct aaa cat tag agg caa c-3′	1549 bp
MCT10	Slc16a10	NM_138831	5′-atg tgg tgc aat ggg tct gt-3′ 5′-cag aat gac cag tga cgg ct-3′	342 bp
MCT11	Slc16a11	NM_001105797	5′-ggg agt cct aac ctc gct tg-3′ 5′-agc taa agg ccg tag caa gg-3′	322 bp
MCT12	Slc16a12	NM_001191637	5′-agc ctt cct tct ttg tgg-3′ 5′-tct gat cta act cct tcg c-3′	179 bp
MCT13	Slc16a13	NM_001005530	5′-gtt tgg gag ccc aat agg ca-3′ 5′-ccc ctc caa gcg tag ttg tt-3′	318 bp
MCT14	Slc16a14	NM_001108229	5′-atc gtg gga cct ttc atc gg-3′ 5′-gct gcc act ccg aag gta at-3′	318 bp
β-actin	–	NM_031144	5′-tca tga agt gtg acg ttg aca tcc gt-3′ 5′-cct aga agc att tgc ggt gca cga tg-3′	285 bp

X. Oocytes Uptake Study

The open reading frame of rat MCT5 (GenBank accession # NM_001013913), MCT8 (GenBank accession # NM_147216), and MCT9 (GenBank accession # NM_017601786) was inserted into a pGEM-HE plasmid, as described previously (22). The capped complementary RNA (cRNA; 2.5 μg/μL) from a *Nhe*I-linearized plasmid was synthesized with a T7 RiboMax™ Large Scale RNA Production System (Promega, Madison, WI, USA) and injected into *X.* oocytes (58 ng/oocyte). Control oocytes were injected with nuclease-free water (23 nL/oocyte). The oocytes were cultivated in Birth's solution (88 mM NaCl, 2.4 mM $NaHCO_3$, 1.0 mM KCl, 0.8 mM $MgSO_4$, 0.4 mM $CaCl_2$, 0.3 mM $Ca(NO_3)_2$, 15 mM Tris-HCl, 2.5 mM pyruvic acid, 100 μg/mL penicillin, and 100 μg/mL streptomycin; pH 7.6) for 3 days. Subsequently, 8–10 oocytes were pre-incubated with ND96 buffer (96 mM NaCl, 2 mM KCl, 1.8 mM $CaCl_2$, 1 mM $MgCl_2$, and 5 mM HEPES–NaOH; pH 7.4) for 5 min at 20°C. Next, the oocytes were treated with 200 μL of 0.1 μCi [^{14}C]phenytoin-containing ND96 buffer (20°C; [^{14}C]phenytoin concentration, 9.09 μM) in the absence or presence of 400 μM unlabeled phenytoin, 1 mM BSP, or 1 mM desipramine. At the designated time points, the oocytes were washed with ice-cold ND96 buffer to terminate the [^{14}C]phenytoin uptake. The oocytes were solubilized with 5% sodium dodecyl sulfate/water. The radioactivity of [^{14}C]phenytoin in the samples was measured using an AccuFLEX LSC-7400 liquid scintillation counter. The uptake activity was expressed as the oocyte/medium ratio (μL/oocyte), which was obtained by dividing the [^{14}C]phenytoin amount in the solubilized sample (pmol/oocyte) by the [^{14}C]phenytoin concentration in the uptake buffer (μM: pmol/μL).

Data and Statistical Analyses

All data were expressed as the mean ± standard deviation (S.D.). Group sizes (n) are reported a number of mice, rats, or oocytes per each group or condition. Statistical differences between the means of two or more than three groups with the same or different n were determined using the unpaired two-tailed Student's t test or one-way analysis of variance, followed by Dunnett's test.

RESULTS

[^{14}C]Phenytoin Efflux Transport across the BBB *In Vivo*

To evaluate the brain-to-blood efflux transport of phenytoin across the BBB, we performed experiments to determine the *in vivo* BEI in rats and mice. After injecting [^{14}C]phenytoin into the rat Par2 region, the 100 − BEI value of [^{14}C]phenytoin decreased in a time-dependent manner with the elimination rate constant $k_{el,\ BBB} = 4.13 \times 10^{-2} \pm 0.46 \times 10^{-2}$ min^{-1} and the half-life $t_{1/2} = 16.8 \pm 1.9$ min (Fig. 1a). The 100 − BEI value of [^{14}C]phenytoin at 30 min was significantly increased after pre-administration of 1 mM unlabeled phenytoin compared to the value for the control (Fig. 1b). In

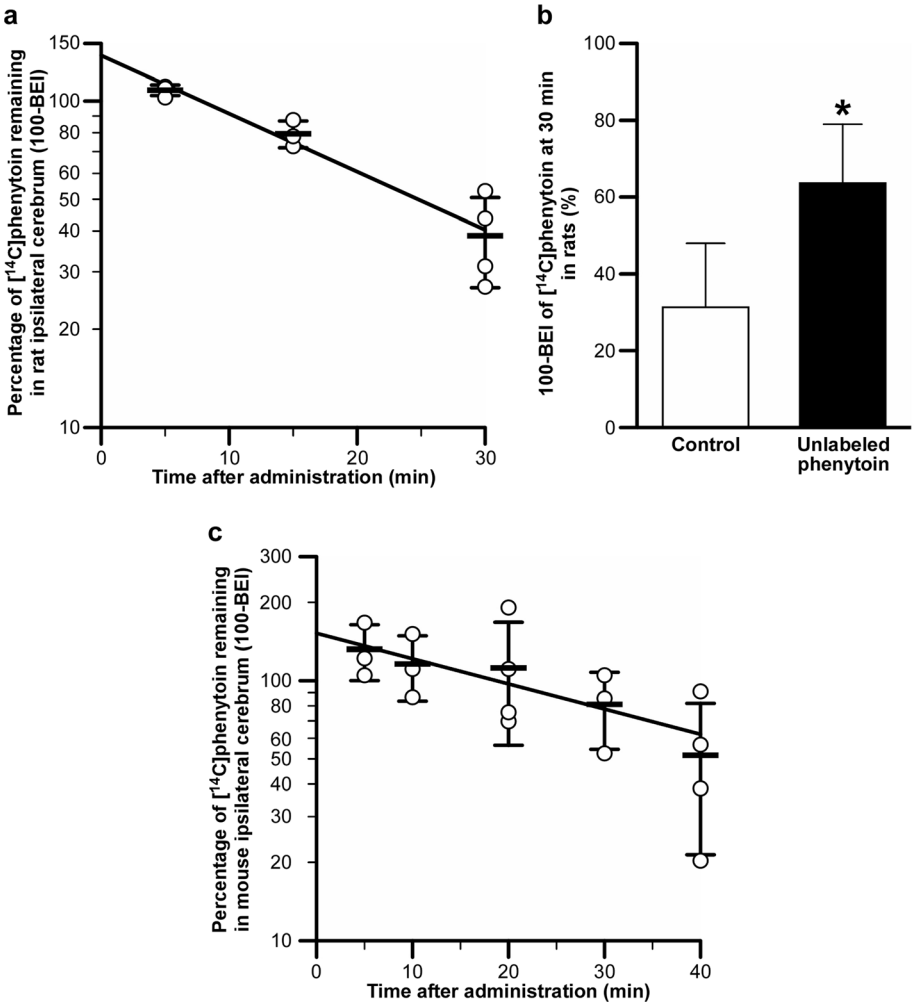

Fig. 1 *In vivo* brain elimination of [^{14}C]phenytoin across the BBB in rats (**a** and **b**) and mice (**c**). (**a**) Time profile of [^{14}C]phenytoin remaining in the rat ipsilateral brain hemisphere after administration of [^{3}H]D-mannitol (0.050 μCi/rat; 8.14 μM) and [^{14}C]phenytoin (0.010 μCi/rat; 364 μM) into the parietal cortex region. Non-linear least-square analysis was used to obtain the line of elimination (solid line). Each open circle represents an individual rat. The data represent the mean ± S.D. (n = 3–4). (**b**) Effect of pre-administering unlabeled phenytoin on [^{14}C]phenytoin levels remaining in the ipsilateral brain hemisphere after 30 min. Following [^{3}H]D-mannitol and [^{14}C]phenytoin intracerebral administration, ECF buffer containing 5% ethanol without (control) or with 1 mM unlabeled phenytoin was administered. Each column represents the mean ± S.D. (n = 4–6). *$p < 0.05$, significantly different from control. (**c**) Time-profile of [^{14}C]phenytoin remaining in the mouse ipsilateral brain hemisphere after administration of [^{3}H]D-mannitol (0.096 μCi/mouse; 26.0 μM) and [^{14}C]phenytoin (0.019 μCi/mouse; 1.15 mM) into the intracerebral somatosensory region. Non-linear least-square analysis was used to obtain the line of elimination (solid line). Each open circle represents an individual rat. The data represent the mean ± S.D. (n = 3–4).

mice, the 100 − BEI value of [^{14}C]phenytoin decreased in a time-dependent manner (Fig. 1c). The brain elimination rate constant of phenytoin in the mice was $k_{el,\ BBB} = 2.23 \times 10^{-2} \pm 0.75 \times 10^{-2}$ min^{-1}, and the half-life of phenytoin in the brain was $t_{1/2} = 31.1 \pm 10.8$ min.

Cerebral Distribution and BBB-Mediated Clearance of [^{14}C]Phenytoin

To obtain the value for phenytoin efflux clearance across the BBB in rats, we determined the brain distribution of phenytoin ($V_{d,\ brain}$) by performing uptake studies using brain slices (Fig. 2). The [^{14}C]phenytoin uptake in rat brain slices increased continuously up to the time point of 60 min. The slice/medium ratio of [^{14}C]phenytoin at 90 min was not significantly different from that at 60 min ($p = 0.510$), and the $V_{d,\ brain}$ for [^{14}C]phenytoin was determined to be 4.28 ± 0.07 mL/g brain (slice/medium ratio at 90 min = 0.125) (16). Using $k_{el,\ BBB}$ and $V_{d,\ brain}$, we determined the elimination clearance of [^{14}C]phenytoin across the BBB as 177 ± 20 µL/(min•g brain).

In Vivo Transport of [^{14}C]Phenytoin across the BBB in mdr1a/1b Knockout Mice

To determine the role of P-gp in the transport of phenytoin across the BBB, we performed *in vivo* transport studies using *mdr1a/1b* knockout mice (Fig. 3). First, in brain perfusion

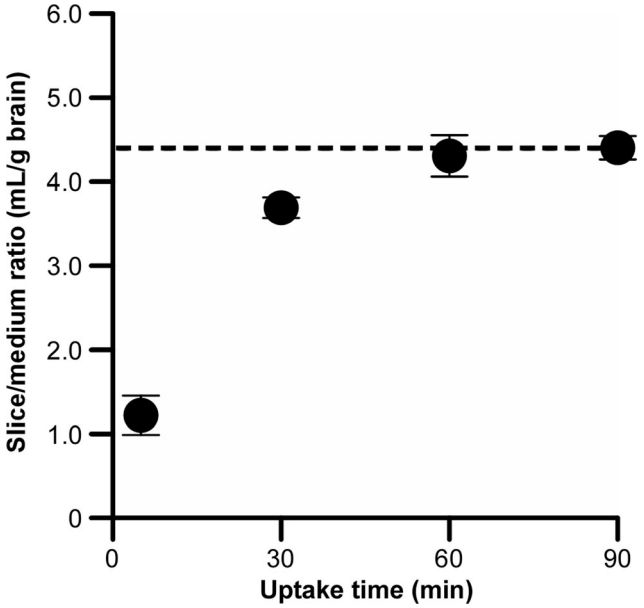

Fig. 2 Time-profile of [^{14}C]phenytoin uptake by rat brain slices. Uptake of [^{14}C]phenytoin (0.2 μCi/mL; 3.64 μM) was measured at the indicated time points. The hatched line indicates the slice/medium ratio at steady state. Each point represents the mean ± S.D. (n = 3–4).

experiments, the K_{in} value for [^{14}C]phenytoin was not significantly different between the wild-type and *mdr1a/1b* knockout mice (Fig. 3a). The vascular integrity of both mouse strains was comparable, as indicated by the [^{3}H]D-mannitol vascular volume (Fig. 3b). Second, in experiments for determining the [^{14}C]phenytoin BEI, we observed that 30 min after the [^{14}C]phenytoin intracerebral injection, the percentage of [^{14}C]phenytoin remaining in the ipsilateral cerebrum of the *mdr1a/1b* knockout mice was not significantly different compared with that of the wild-type mice (Fig. 3c). These results indicate that P-gp affects neither the influx nor efflux transport of phenytoin across the mouse BBB.

Inhibition of [^{14}C]Phenytoin Efflux Transport

To identify the transporter involved in phenytoin efflux transport across the BBB, we evaluated the effect of pre-administration of several drugs and compounds that modulate various transporters on the [^{14}C]phenytoin BEI (30 min time point; Table II). Pre-administration of 20 mM BSP, a known substrate/inhibitor of MRPs and MCT8 (15, 23), significantly decreased the [^{14}C]phenytoin BEI by 82%. Additionally, the [^{14}C]phenytoin BEI was significantly decreased with the pre-administration of 20 mM desipramine, which inhibits MCT8 and MCT10 (15), as well as cationic drug-sensitive transport processes at the BBB (10). In contrast, the [^{14}C]phenytoin BEI was not significantly altered by 5 mM quinidine or 4 mM verapamil, which are both inhibitors of cationic drug-sensitive transport processes at the BBB and P-gp substrates (10, 24). Moreover, pre-administration of PSC833, a typical inhibitor for P-gp (24), did not alter the [^{14}C]phenytoin BEI. As with inhibitors against the other transporters, the [^{14}C]phenytoin BEI was not significantly altered with the pre-administration of 20 mM probenecid (MRP and MCT6 inhibitor), 500 µM prazosin (BCRP substrate), 20 mM MK-571 (MRP inhibitor), 10 mM methotrexate (MRP and BCRP substrate), or 10 mM dehydroepiandrosterone sulfate (DHEAS; MRP and BCRP substrate) (9, 25–28) Fig. 4.

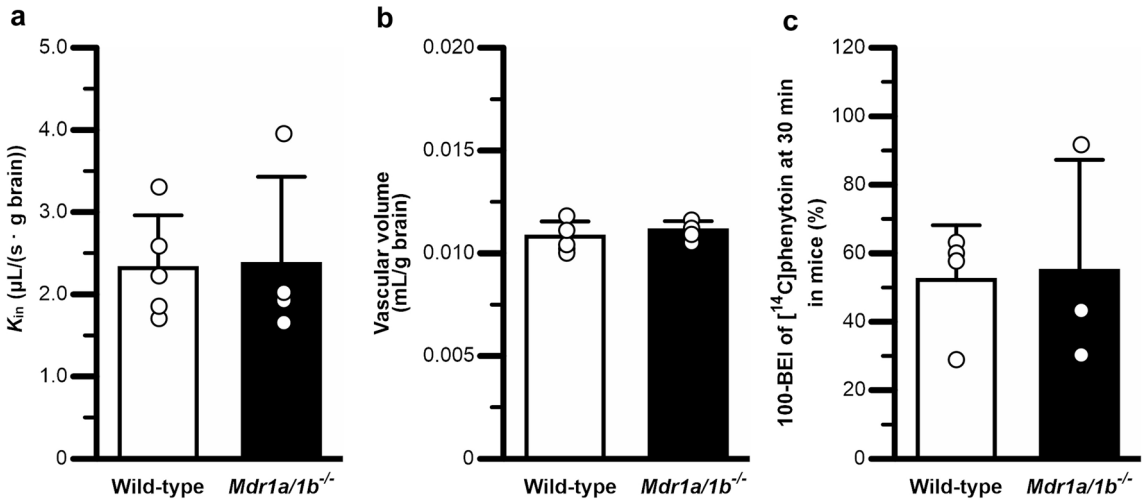

Fig. 3 Influx (**a** and **b**) and efflux transport (**c**) of phenytoin across the BBB in mdr1a/1b knockout mice. (**a**) and (**b**) *In situ* brain perfusion of [^{14}C]phenytoin (0.15 μCi/mL; 2.73 μM) was performed at 2.5 mL/min for 2 min in wild-type and *mdr1a/1b* knockout (*Mdr1a/1b*$^{-/-}$) mice (**a**). [^{3}H]D-mannitol was used to determine the vascular volume (**b**). Each open circle represents an individual mouse. Each column represents the mean ± S.D. (n = 4–5). (**c**) No significant difference in the 100 − BEI values for [^{14}C]phenytoin between the wild-type and *mdr1a/1b* knockout mice 30 min after intracerebral administration of [^{3}H]D-mannitol (0.096 μCi/mouse; 26.0 μM) and [^{14}C]phenytoin (0.019 μCi/mouse; 1.15 mM). Each open circle represents an individual mouse. Each column represents the mean ± S.D. (n = 3–4).

Table II Effect of Pre-Administration of Compounds on [^{14}C]phenytoin Efflux Across the rat BBB

Compound	Concentration (mM)	BEI (%)	% of Control
Control		64.1 ± 12.9	100 ± 20
BSP	20	11.9 ± 10.3	18.5 ± 16.1**
Desipramine	20	28.4 ± 20.7	44.3 ± 32.3**
Quinidine	5	50.5 ± 13.1	78.8 ± 20.4
Verapamil	4	74.4 ± 8.3	116 ± 13
Probenecid	20	56.5 ± 24.9	88.1 ± 38.8
Prazosin	0.5	59.4 ± 8.5	92.7 ± 13.3
MK-571	20	64.4 ± 6.7	100 ± 10
Methotrexate	10	67.3 ± 16.7	105 ± 26
DHEAS	10	77.9 ± 11.3	121 ± 18
Control (0.1% DMSO)		53.4 ± 14.3	100 ± 27
PSC833 (0.1% DMSO)	0.004	53.3 ± 3.5	100 ± 7

Fifty microliters of ECF buffer (control) or ECF buffer containing the respective compounds at the indicated concentration with or without 0.1% DMSO were pre-administered into the ipsilateral brain hemisphere 5 min prior to the intracerebral injection (0.5 μL) of [^{14}C]phenytoin (0.1 μCi/rat) and [^{3}H]D-mannitol (0.5 μCi/rat). Each value represents the mean ± S.D. (n = 3–23). **$p < 0.01$, significantly different from control. *BSP* bromosulfophthalein, *DHEAS* dehydroepiandrosterone sulfate

Expression of Orphan Monocarboxylate Transporters in Brain Capillaries

Orphan monocarboxylate transporters (MCTs), specifically MCT5 and MCT7 (13), are potential candidates for the mediation of phenytoin efflux transport at the BBB. We, therefore, performed RT-PCR to determine the mRNA expression profile of orphan MCTs at the BBB (Fig. 5). We utilized cDNA samples from the rat brain capillaries, as well as those from the liver and kidney, as positive controls; β-actin was run as a technical positive control and detected at 285 bp in all rat tissue samples. We observed mRNA expression for MCT5 (981 bp), MCT8 (310 bp), and MCT9 (1549 bp) in the rat brain capillaries. In contrast, the bands corresponding to MCT7, MCT10, MCT11, MCT12, MCT13, and MCT14 were observed in the positive controls (rat liver: MCT7, MCT10, MCT11, and MCT13; rat kidney: MCT12 and MCT14) but not in the rat brain capillaries.

We additionally examined the mRNA expression of MCT8 in the mouse brain capillaries and MCT8 protein expression in the rat brain capillaries. Amplified products derived from MCT8 (310 bp) in addition to β-actin (285 bp) were detected in the sample of mouse brain capillaries, as well as in that of the whole brain used as a positive control (Fig. 6). Moreover, MCT8- and Na^+, K^+-ATPase α1-derived immunoreactivities were observed at ~60 kDa (14) and ~ 110 kDa, respectively (21), in the Western blot analysis, using the crude membrane fraction of the rat brain capillaries in addition to rat liver used as a positive control (29, 30), indicating the protein expression of MCT8 in the brain capillaries (Fig. 7).

[^{14}C]Phenytoin Uptake by MCT-Expressing X. Oocytes

To determine whether one of the three MCTs (MCT5, MCT8, or MCT9) detected in the rat brain capillaries could transport phenytoin, we conducted uptake studies with *X. oocytes* expressing MCT5, MCT8, or MCT9. The [^{14}C]phenytoin uptake by the *X. oocytes* expressing MCT5 or MCT9 was not significantly different compared to the [^{14}C]phenytoin uptake by the water-injected *X. oocytes* (Figs. 8a and c). In contrast, the [^{14}C]phenytoin uptake by the MCT8-expressing oocytes was 1.5-fold greater than that by the water-injected *X. oocytes* (Fig. 8b). In the presence of 400 μM unlabeled phenytoin, 1 mM BSP, and 1 mM desipramine, the [^{14}C]phenytoin oocyte/medium ratio in the MCT8-expressing *X. oocytes* was not significantly different from that in the water-injected *X. oocytes*, indicating that MCT8 was responsible for the [^{14}C]phenytoin uptake.

DISCUSSION

The objective of this study was to investigate in detail the transport kinetics of phenytoin across the BBB. Here, we demonstrated the carrier-mediated brain-to-blood transport of phenytoin across the BBB (Figs. 1 and 2). Our data indicate that P-gp plays a minor role, if any, in phenytoin efflux transport (Table II and Fig. 3). In addition, on the basis of our *in vivo* and *in vitro* studies (Table II and Figs. 5, 6, 7 and 8), we propose that MCT8 is a possible candidate for mediating phenytoin efflux transport across the BBB. Several aspects of our study require additional discussion.

First, we demonstrated that [^{14}C]phenytoin injected into the cerebral cortex was eliminated with a half-life of 17 min in rats and 31 min in mice (Fig. 1a and c). In addition, our uptake studies with the rat brain slices (Fig. 2) demonstrated that the cerebral elimination clearance of phenytoin across the rat BBB was 177 μL/(min·g brain). In this regard, Cornford *et al.* conducted brain uptake index studies in adult rats and determined that the blood-to-brain influx clearance of phenytoin was 64 μL/(min·g brain) (7). Since the phenytoin elimination clearance determined in our study is 2.8-fold greater than the phenytoin influx clearance determined by Cornford *et al.*, the net phenytoin flux across the BBB appears to represent the brain-to-blood efflux transport.

Second, our data indicated that the unlabeled phenytoin reduced [^{14}C]phenytoin efflux transport (Fig. 1b), which suggests that phenytoin efflux transport across the BBB is carrier-mediated. Several previous reports have discussed the role of P-gp in determining the brain levels of phenytoin following

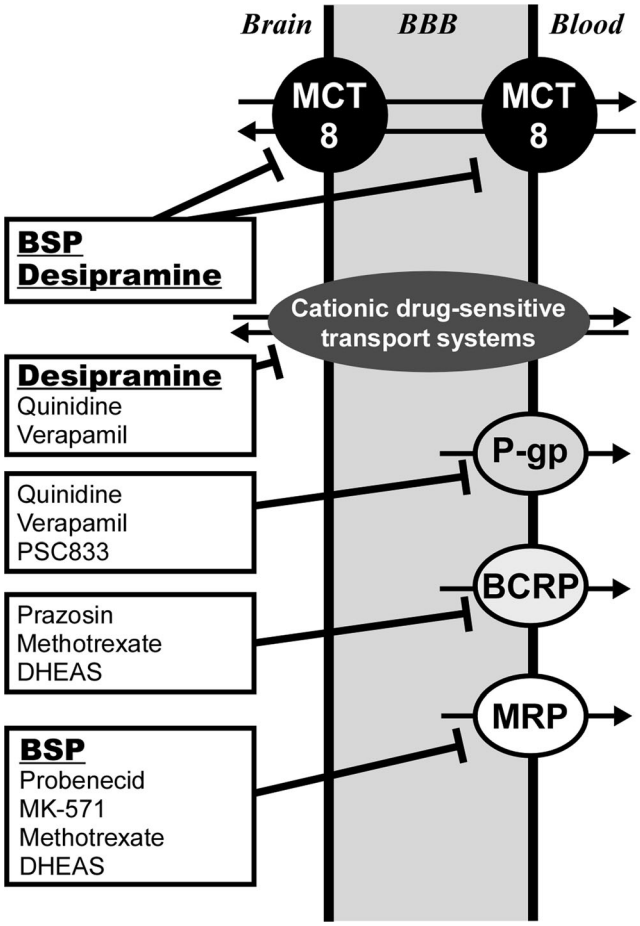

Fig. 4 Schematic diagram of BBB transporters with the sites of interaction for inhibitors used in this study. The interaction of inhibitors with the transporters is detailed in the Result and Discussion sections. The compound with an underline exhibited significant inhibition of [^{14}C]phenytoin efflux transport across the BBB, as shown in Table II. BBB, blood-brain barrier; BCRP, breast cancer resistance protein; BSP, bromosulfophthalein; DHEAS, dehydroepiandrosterone-3-sulfate; MCT, monocarboxylate transporter; MRP, multidrug resistance-associated protein; P-gp, P-glycoprotein.

peripheral administration (11, 12, 31). Kusuhara *et al.* conducted BEI studies with pre-administration of 5 mM unlabeled quinidine and 4 mM verapamil and demonstrated P-gp involvement in [^{3}H]quinidine efflux transport (24). In our present study, however, pre-administration of unlabeled transporter inhibitors exhibited little effect on [^{14}C]phenytoin efflux transport (Table II). In addition, the *in situ* brain perfusion and BEI studies in P-gp-deficient mice revealed that neither the influx nor efflux transport of phenytoin was affected (Fig. 3). These data suggest that P-gp plays a minor role, if any, in phenytoin efflux transport across the BBB.

Third, our results suggest that BCRP and MRP play no role in brain phenytoin clearance via the BBB. Intracerebral pre-administration of BCRP substrates, such as prazosin and methotrexate (9), exhibited essentially no effect on phenytoin efflux transport across the rat BBB (Table II). Reports show that phenytoin is metabolized by CYP2C9 and CYP2C19 and is subsequently converted into its glucuronide metabolites (4). Several drug-glucuronides are actively transported by MRP2 and MRP4, both of which are expressed at the BBB (9, 32). BSP, probenecid, methotrexate, and DHEAS are known substrates for MRP2 and/or MRP4 (23, 25, 28), and phenytoin efflux transport was significantly decreased after BSP pre-administration (Table II). However, probenecid, MK-571, methotrexate, and DHEAS did not affect phenytoin efflux transport (Table II), suggesting that MRP2 and MRP4 are not involved in the efflux transport of phenytoin and its metabolites in the brain. Nevertheless, several reports claim that a putative transport system(s) that recognize(s) cationic drugs is/are present at the BBB and is/are involved in brain drug distribution (10). For example, it has been reported that this putative transport system(s) is/are inhibited by desipramine, quinidine, and verapamil (10). As shown in Table II, pre-administration of desipramine significantly inhibited phenytoin efflux transport across the BBB, whereas quinidine and verapamil exhibited little effect. Our data suggest only a minor contribution of BCRP, MRP2/4, and the putative cationic drug transport system(s) to phenytoin efflux transport.

Fourth, we show that both BSP and desipramine (MCT8 and/or MCT10 inhibitors) inhibited phenytoin efflux across the BBB (Table II). Among all MCTs, MCT1–4 are transporters for monocarboxylates, such as L-lactate (33). However, other compounds transported by MCTs that are not monocarboxylates are, therefore, referred to as "orphan" MCTs (34). Our mRNA expression data using rat brain capillaries indicate that MCT5, MCT8, and MCT9 mRNAs are expressed at the rat BBB (Fig. 5). Among these MCTs, it is strongly suggested that MCT8 is expressed in the mouse/rat BBB, according to the mouse RT-PCR studies in mice and Western blot analyses in rats (Figs. 6 and 7). Moreover, our data show that phenytoin uptake only occurs in *X.* oocytes over-expressing MCT8 but not in those over-expressing MCT5 or MCT9 (Fig. 8). Interestingly, the [^{14}C]phenytoin uptake by MCT8-expressing *X.* oocytes was attenuated in the presence of BSP and desipramine (Fig. 8b), which are reported to inhibit MCT8-mediated transport of the other substrates by more than 50% at a concentration of 1 mM (15). Considering our data and the observation that probenecid (MCT6 inhibitor) did not inhibit phenytoin efflux transport (Table II) (27), we propose that MCT8 is the phenytoin efflux transporter at the BBB. The mRNA/protein expression level of MCT8 has not been compared with that of other transporters at the BBB. Determination of the absolute expression of transporters at the BBB would clarify, in detail, the role of MCT8 in phenytoin efflux transport across the BBB. Roberts *et al.* reported that MCT8 is localized on both luminal and abluminal membranes of the rat BBB (14). Hence, it is conceivable that MCT8 contributes to the blood-to-brain influx transport of phenytoin across the BBB

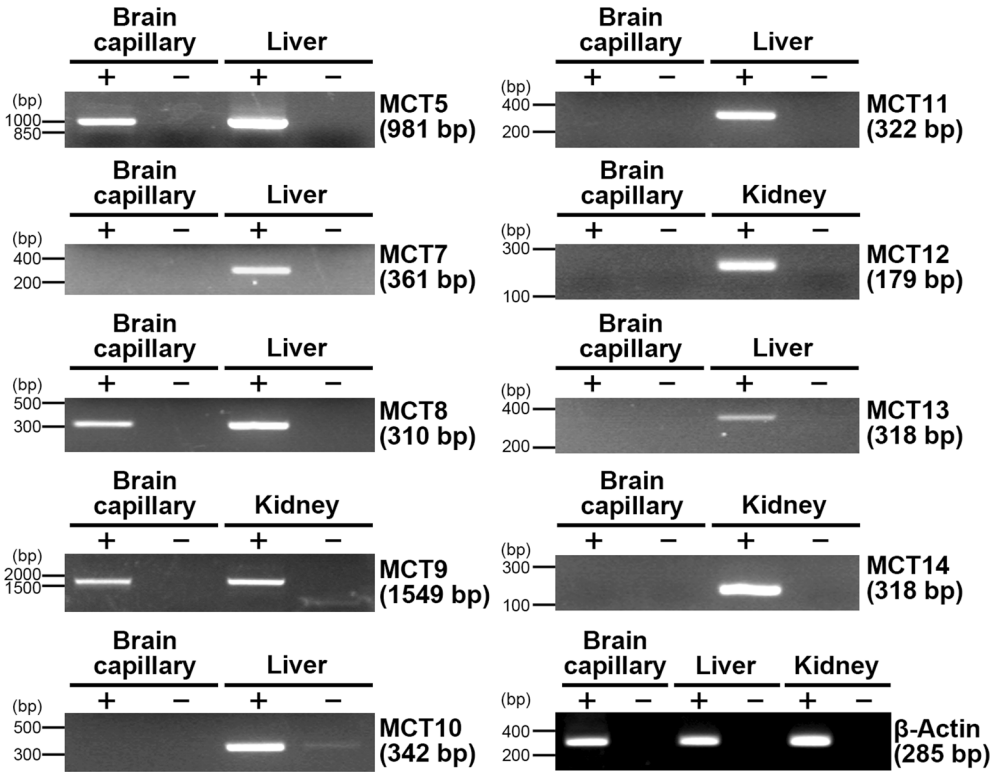

Fig. 5 mRNA expression of monocarboxylate transporters in rat brain capillaries. RT-PCR was performed in the absence (−) or presence (+) of reverse transcriptase. Total RNA from the rat liver and kidney was used as a positive control for mRNA expression. This image was representative of the images from 3 replicates.

as well. Because this study was limited to chemical inhibition studies, the contribution of MCT8 to phenytoin transport across the BBB has not been fully determined. This contribution could be elucidated using MCT8-gene-deficient animals in future studies. Nevertheless, through our *in vivo* and *in vitro* studies, we suggest that MCT8 participates in the phenytoin efflux transport system(s) at the BBB.

Fifth, our study demonstrated the characteristics of *in vivo* phenytoin efflux transport across the BBB in male animals and the possible involvement of MCT8 in its efflux transport (Fig. 1 and Table II). In fathead minnows, the MCT8 mRNA level in the adult female gonad was reported to be significantly greater than that in the adult male gonad (35). Thus, the possibility that the expression levels of MCT8 at the BBB and activities of BBB-mediated phenytoin efflux transport are different between the male and female animals is not negligible. In contrast, it is possible that the age of the animals is not crucial for the alteration of MCT8-mediated phenytoin transport, because Wilpert *et al.* recently reported that the MCT8 protein level in the cerebral endothelial cells of P83 mice is unaltered compared with that in P6, P12, and P21 mice (36). The appropriate use of phenytoin, considering its cerebral distribution, could be established through further in vivo analyses using male and female mice/rats of various ages.

Lastly, to the best of our knowledge, it has never been demonstrated that MCT8 expression and activity levels are associated with the brain distribution and pharmacology of

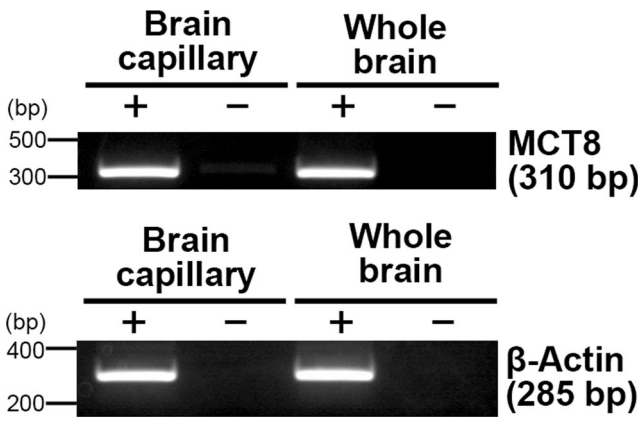

Fig. 6 Expression of monocarboxylate transporter 8 (MCT8) mRNA in mouse brain capillaries. RT-PCR was performed in the absence (−) or presence (+) of reverse transcriptase. Total RNA from the mouse brain was used as a positive control for MCT8 mRNA expression. This image was representative of the images from 3 replicates.

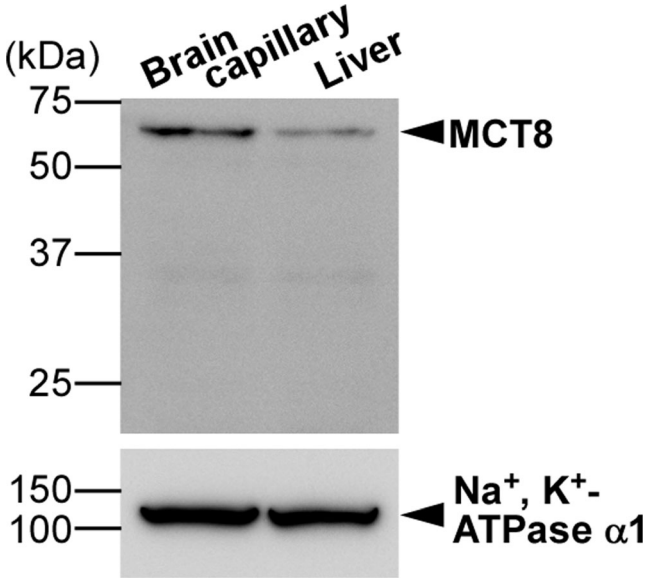

Fig. 7 Protein expression of monocarboxylate transporter 8 (MCT8) in rat brain capillaries. Crude membrane fraction (25 μg) from rat brain capillaries and liver was used for the Western blot analysis of MCT8 proteins. Na^+, K^+-ATPase α1 was used for the loading control of the crude membrane fraction (21). An arrowhead indicates the expected size of the rat MCT8 proteins (14).

drugs including phenytoin. The blood-cerebrospinal fluid barrier (BCSFB) is widely regarded as the other brain barrier. Our BEI study of phenytoin (Fig. 1 and Table II) did not reflect BCSFB-mediated efflux transport because it has been reported that the injectate at a volume of 0.5 µL hardly diffuses to the CSF (16). However, Müller and Heuer have reported that MCT8 is also expressed in the BCSFB (37). Hence, *in vivo* studies on BCSFB-mediated phenytoin transport in the future could lead to a deep understanding of the role of brain barriers in cerebral phenytoin distribution. Our results indicate, for the first time, that MCT8 transports an "exogeneous" compound. In contrast, thyroid hormones are endogenous MCT8 substrates, and one single nucleotide polymorphism (SNP) in MCT8 has been reported to alter the blood levels of triiodothyronine (29, 38). In addition, Mayerl *et al.* have shown that MCT8 deficiency alters brain triiodothyronine levels in mice (39), and phenytoin administration causes hypothyroidism as an adverse effect (40). Hence, it is conceivable that MCT8 affects the pharmacokinetics of phenytoin. Additionally, reports have indicated that MCT8 is expressed in several peripheral tissues, such as the heart, liver, and kidney (29). Considering that our data demonstrate MCT8 inhibition using unlabeled phenytoin (Fig. 5b), it is possible that phenytoin might affect the blood and tissue levels of the thyroid hormone and, in turn, the dynamics and effects of the thyroid hormone. However, for fully supporting this theory, additional studies will be required.

In summary, we demonstrate phenytoin efflux transport across the BBB. Our data suggest that MCT8 transports phenytoin, participates in phenytoin efflux transport across the BBB, and plays a more prominent role in phenytoin efflux compared to ABC transporters such as P-gp. Thus, our study implies that MCT8 is a key transporter involved in phenytoin BBB transport. Our findings are expected to improve the understanding of phenytoin kinetics and, thus, support the development of treatment regimens utilizing phenytoin for refractory epilepsy.

ACKNOWLEDGMENTS AND DISCLOSURES

The authors thank Mr. Kosuke Tajima (University of Toyama) for helping with the mRNA expression analysis for MCTs. This research was supported by The Mochida Memorial Foundation for Medical and Pharmaceutical Research, The Research Foundation for Pharmaceutical Sciences, and Japan Society for the Promotion of Science (JSPS) KAKENHI [Grant Numbers JP16K08365 (to S.A.), JP16H05110 (to K.H.), and JP19K07160 (to S.A.)]. This project was also supported by Grant 1R01NS079507 from the

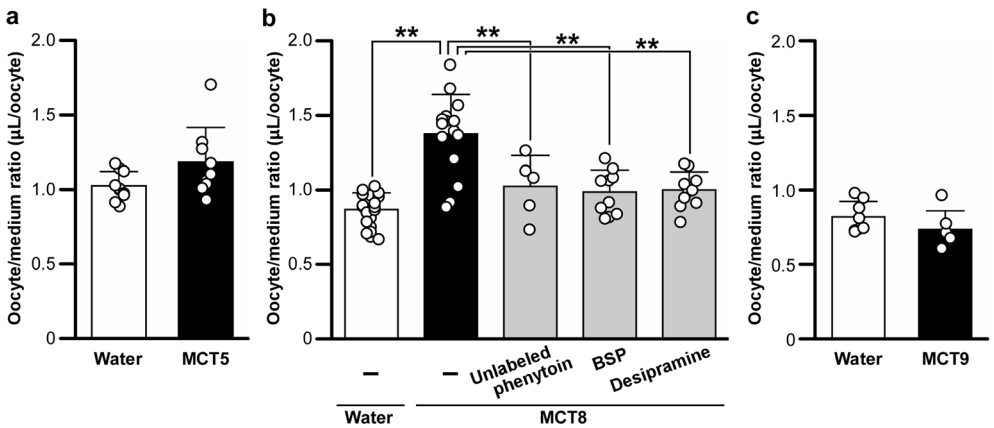

Fig. 8 [^{14}C]Phenytoin uptake in X. oocytes expressing MCT5 (**a**), MCT8 (**b**), or MCT9 (**c**). [^{14}C]Phenytoin uptake (0.1 μCi/200 μL; 9.09 μM) in *X. oocytes* expressing rat MCT5 (**a**), MCT8 (**b**), or MCT9 (**c**) or in *X. oocytes* injected with nuclease-free water (**a**, **b**, and **c**) in the absence (−, **b**) or presence of 400 μM unlabeled phenytoin, 1 mM bromosulfophthalein (BSP), or 1 mM desipramine (**b**). Each open circle represents an individual sample. Each column represents the mean ± S.D. (n = 5–20). **$p < 0.01$, a significant difference.

U.S. National Institutes of Health (NIH)/National Institute of Neurological Disorders and Stroke (to B.B.). The content is solely the responsibility of the authors, and it does not necessarily represent the official views of the National Institute of Neurological Disorders and Stroke or the NIH. All authors declare no conflict of interest.

AUTHOR CONTRIBUTIONS

R.J., S.A., B.B., and Y.Y. performed the experiments; R.J., S.A., B.B., Y.K., and H.K. designed the experiments and analyzed the data.; and R.J. and S.A. wrote the manuscript. All authors read the final version of the manuscript.

REFERENCES

1. Zeng Z, Hill-Yardin EL, Williams D, O'Brien T, Serelis A, French CR. Effect of phenytoin on sodium conductances in rat hippocampal CA1 pyramidal neurons. J Neurophysiol. 2016;116(4):1924–36.
2. Carter CH. Use of parenteral diphenylhydantoin (dilantin) sodium in control of status epilepticus. AMA Arch Neurol Psychiatry. 1958;79(2):136–7.
3. Kwan P, Brodie MJ. Early identification of refractory epilepsy. N Engl J Med. 2000;342(5):314–9.
4. Bajpai M, Roskos LK, Shen DD, Levy RH. Roles of cytochrome P4502C9 and cytochrome P4502C19 in the stereoselective metabolism of phenytoin to its major metabolite. Drug Metab Dispos. 1996;24(12):1401–3.
5. Fohner AE, Ranatunga DK, Thai KK, Lawson BL, Risch N, Oni-Orisan A, *et al.* Assessing the clinical impact of CYP2C9 pharmacogenetic variation on phenytoin prescribing practice and patient response in an integrated health system. Pharmacogenet Genomics. 2019;29(8):192–9.
6. Ramasamy K, Narayan SK, Shewade DG, Chandrasekaran A. Influence of CYP2C9 genetic polymorphism and undernourishment on plasma-free phenytoin concentrations in epileptic patients. Ther Drug Monit. 2010;32(6):762–6.
7. Cornford EM, Pardridge WM, Braun LD, Oldendorf WH. Increased blood–brain barrier transport of protein-bound anticonvulsant drugs in the newborn. J Cereb Blood Flow Metab. 1983;3(3):280–6.
8. Sadiq MW, Boström E, Keizer R, Bjorkman S, Hammarlund-Udenaes M. Oxymorphone active uptake at the blood–brain barrier and population modeling of its pharmacokinetic–Pharmacodynamic relationship. J Pharm Sci. 2013;102(9):3320–31.
9. Ohtsuki S, Terasaki T. Contribution of carrier-mediated transport systems to the blood-brain barrier as a supporting and protecting interface for the brain; importance for CNS drug discovery and development. Pharm Res. 2007;24(9):1745–58.
10. Okura T, Hattori A, Takano Y, Sato T, Hammarlund-Udenaes M, Terasaki T, *et al.* Involvement of the pyrilamine transporter, a putative organic cation transporter, in blood-brain barrier transport of oxycodone. Drug Metab Dispos. 2008;36(10):2005–13.
11. Potschka H, Loscher W. In vivo evidence for P-glycoprotein-mediated transport of phenytoin at the blood-brain barrier of rats. Epilepsia. 2001;42(10):1231–40.
12. Schinkel AH, Wagenaar E, Mol CA, van Deemter L. P-glycoprotein in the blood-brain barrier of mice influences the brain penetration and pharmacological activity of many drugs. J Clin Invest. 1996;97(11):2517–24.
13. Felmlee MA, Jones RS, Rodriguez-Cruz V, Follman KE, Morris ME. Monocarboxylate transporters (SLC16): function, regulation, and role in health and disease. Pharmacol Rev. 2020;72(2):466–85.
14. Roberts LM, Woodford K, Zhou M, Black DS, Haggerty JE, Tate EH, *et al.* Expression of the thyroid hormone transporters monocarboxylate transporter-8 (SLC16A2) and organic ion transporter-14 (SLCO1C1) at the blood-brain barrier. Endocrinology. 2008;149(12):6251–61.
15. Roth S, Kinne A, Schweizer U. The tricyclic antidepressant desipramine inhibits T3 import into primary neurons. Neurosci Lett. 2010;478(1):5–8.
16. Kakee A, Terasaki T, Sugiyama Y. Brain efflux index as a novel method of analyzing efflux transport at the blood-brain barrier. J Pharmacol Exp Ther. 1996;277(3):1550–9.
17. Akanuma S, Ohtsuki S, Doi Y, Tachikawa M, Ito S, Hori S, *et al.* ATP-binding cassette transporter A1 (ABCA1) deficiency does not attenuate the brain-to-blood efflux transport of human amyloid-beta peptide (1-40) at the blood-brain barrier. Neurochem Int. 2008;52(6):956–61.
18. Akanuma S, Higuchi T, Higashi H, Ozeki G, Tachikawa M, Kubo Y, *et al.* Transporter-mediated prostaglandin E(2) elimination across the rat blood-brain barrier and its attenuation by the activation of N-methyl-D-aspartate receptors. Drug Metab Pharmacokinet. 2014;29(5):387–93.
19. Urayama A, Grubb JH, Sly WS, Banks WA. Pharmacologic manipulation of lysosomal enzyme transport across the blood-brain barrier. J Cereb Blood Flow Metab. 2016;36(3):476–86.
20. Soldner ELB, Hartz AMS, Akanuma SI, Pekcec A, Doods H, Kryscio RJ, *et al.* Inhibition of human microsomal PGE2 synthase-1 reduces seizure-induced increases of P-glycoprotein expression and activity at the blood-brain barrier. FASEB J. 2019;33(12):13966–81.
21. Akanuma SI, Yamakoshi A, Sugouchi T, Kubo Y, Hartz AMS, Bauer B, *et al.* Role of L-type amino acid transporter 1 at the inner blood-retinal barrier in the blood-to-retina transport of gabapentin. Mol Pharm. 2018;15(6):2327–37.
22. Akanuma S, Kida R, Tsuchiyama A, Tachikawa M, Kubo Y, Hosoya K. Organic anion-transporting polypeptide 1a4-mediated heterogeneous distribution of sulforhodamine-101 in rat hepatic lobules. Drug Metab Pharmacokinet. 2019;34(4):239–46.
23. Cui Y, Konig J, Keppler D. Vectorial transport by double-transfected cells expressing the human uptake transporter SLC21A8 and the apical export pump ABCC2. Mol Pharmacol. 2001;60(5):934–43.
24. Kusuhara H, Suzuki H, Terasaki T, Kakee A, Lemaire M, Sugiyama Y. P-glycoprotein mediates the efflux of quinidine across the blood-brain barrier. J Pharmacol Exp Ther. 1997;283(2):574–80.
25. Grube M, Hagen P, Jedlitschky G. Neurosteroid transport in the brain: role of ABC and SLC transporters. Front Pharmacol. 2018;9:354.
26. Matsson P, Pedersen JM, Norinder U, Bergstrom CA, Artursson P. Identification of novel specific and general inhibitors of the three major human ATP-binding cassette transporters P-gp, BCRP and MRP2 among registered drugs. Pharm Res. 2009;26(8):1816–31.
27. Murakami Y, Kohyama N, Kobayashi Y, Ohbayashi M, Ohtani H, Sawada Y, *et al.* Functional characterization of human monocarboxylate transporter 6 (SLC16A5). Drug Metab Dispos. 2005;33(12):1845–51.
28. Zamek-Gliszczynski MJ, Xiong H, Patel NJ, Turncliff RZ, Pollack GM, Brouwer KL. Pharmacokinetics of 5 (and 6)-carboxy-2′,7′-dichlorofluorescein and its diacetate promoiety in the liver. J Pharmacol Exp Ther. 2003;304(2):801–9.

29. Friesema EC, Ganguly S, Abdalla A, Manning Fox JE, Halestrap AP, Visser TJ. Identification of monocarboxylate transporter 8 as a specific thyroid hormone transporter. J Biol Chem. 2003;278(41): 40128–35.
30. Schutkowski A, Wege N, Stangl GI, Konig B. Tissue-specific expression of monocarboxylate transporters during fasting in mice. PLoS One. 2014;9(11):e112118.
31. Bankstahl M, Klein S, Romermann K, Loscher W. Knockout of P-glycoprotein does not alter antiepileptic drug efficacy in the intrahippocampal kainate model of mesial temporal lobe epilepsy in mice. Neuropharmacology. 2016;109:183–95.
32. El-Sheikh AA, Koenderink JB, Wouterse AC, van den Broek PH, Verweij VG, Masereeuw R, *et al.* Renal glucuronidation and multidrug resistance protein 2−/ multidrug resistance protein 4-mediated efflux of mycophenolic acid: interaction with cyclosporine and tacrolimus. Transl Res. 2014;164(1):46–56.
33. Vijay N, Morris ME. Role of monocarboxylate transporters in drug delivery to the brain. Curr Pharm Des. 2014;20(10):1487–98.
34. Fisel P, Schaeffeler E, Schwab M. Clinical and functional relevance of the monocarboxylate transporter family in disease pathophysiology and drug therapy. Clin Transl Sci. 2018;11(4):352–64.
35. Muzzio AM, Noyes PD, Stapleton HM, Lema SC. Tissue distribution and thyroid hormone effects on mRNA abundance for membrane transporters Mct8, Mct10, and organic anion-transporting polypeptides (Oatps) in a teleost fish. Comp Biochem Physiol A Mol Integr Physiol. 2014;167:77–89.
36. Wilpert NM, Krueger M, Opitz R, Sebinger D, Paisdzior S, Mages B, *et al.* Spatiotemporal changes of cerebral monocarboxylate transporter 8 expression. Thyroid. 2020;30(9):1366–83.
37. Muller J, Heuer H. Expression pattern of thyroid hormone transporters in the postnatal mouse brain. Front Endocrinol (Lausanne). 2014;5:92.
38. Roef GL, Rietzschel ER. De Meyer T, Bekaert S, De Buyzere ML, Van daele C, Toye K, Kaufman JM, Taes YE. Associations between single nucleotide polymorphisms in thyroid hormone transporter genes (MCT8, MCT10 and OATP1C1) and circulating thyroid hormones. Clin Chim Acta. 2013;425:227–32.
39. Mayerl S, Muller J, Bauer R, Richert S, Kassmann CM, Darras VM, *et al.* Transporters MCT8 and OATP1C1 maintain murine brain thyroid hormone homeostasis. J Clin Invest. 2014;124(5): 1987–99.
40. Miyake Z, Ishii K, Tamaoka A. Hypothyroidism induced by phenytoin and gabapentin: a case report. Medicine (Baltimore). 2018;97(43):e12938.